Contents lists available at ScienceDirect

Materials Science & Engineering C

journal homepage: www.elsevier.com

Development of solvent-casting particulate leaching (SCPL) polymer scaffolds as improved three-dimensional supports to mimic the bone marrow niche

Antonella Sola[a,*], Jessika Bertacchini[b], Daniele D'Avella[c], Laura Anselmi[c], Tullia Maraldi[c], Sandra Marmiroli[c], Massimo Messori[a]

[a] Dipartimento di Ingegneria "Enzo Ferrari" (DIEF), Università di Modena e Reggio Emilia, Via P. Vivarelli, 10, 41125 Modena, Italy
[b] Dipartimento di Scienze Biomediche, Metaboliche e Neuroscienze, Università di Modena e Reggio Emilia, Via del Pozzo, 71, 41124 Modena, Italy
[c] Dipartimento Chirurgico, Medico, Odontoiatrico e di Scienze Morfologiche con interesse Trapiantologico, Oncologico e di Medicina Rigenerativa, Università di Modena e Reggio Emilia, Via del Pozzo, 71, 41124 Modena, Italy

ARTICLE INFO

Keywords:
Three-dimensional supports
Bone marrow niche
Solvent-casting particulate-leaching
Porosity
Pro-survival effect

ABSTRACT

The need for new approaches to investigate *ex vivo* the causes and effects of tumor and to achieve improved cancer treatments and medical therapies is particularly urgent for malignant pathologies such as lymphomas and leukemias, whose tissue initiator cells interact with the stroma creating a three-dimensional (3D) protective environment that conventional mono- and bi-dimensional (2D) models are not able to simulate realistically. The solvent-casting particulate leaching (SCPL) technique, that is already a standard method to produce polymer-based scaffolds for bone tissue repair, is proposed here to fabricate innovative 3D porous structures to mimic the bone marrow niche *in vitro*. Two different polymers, namely a rigid polymethyl methacrylate (PMMA) and a flexible polyurethane (PU), were evaluated to the purpose, whereas NaCl, in the form of common salt table, resulted to be an efficient porogen. The adoption of an appropriate polymer-to-salt ratio, experimentally defined as 1:4 for both PMMA and PU, gave place to a rich and interconnected porosity, ranging between 82.1 vol% and 91.3 vol%, and the choice of admixing fine-grained or coarse-grained salt powders allowed to control the final pore size. The mechanical properties under compression load were affected both by the polymer matrix and by the scaffold's architecture, with values of the elastic modulus indicatively varying between 29 kPa and 1283 kPa. Preliminary tests performed with human stromal HS-5 cells co-cultured with leukemic cells allowed us to conclude that stromal cells grown associated to the supports keep their well-known protective and pro-survival effect on cancer cells, indicating that these devices can be very useful to mimic the bone marrow microenvironment and therefore to assess the efficacy of novel therapies in pre-clinical studies.

1. Introduction

The conventional approach to develop therapies against cancer makes use of bi-dimensional (2D) tissue cultures, where tumor cells are seeded, grown and tested on mono- and bi-dimensional substrata. Even if their complexity greatly depends on their objectives, such models often fail to reproduce the micro-environment existing *in vivo*, that is instead an evolving and three-dimensional structure [1–4]. On the other hand, animal models, besides requiring specific facilities and posing ethical concerns, often provide a limited understanding of the individual steps of the metastatic process and suffer from a problematic determination of quantitative mechanistic data [4,5]. The inadequacy of standard methods is particularly striking for malignant pathologies such as leukemias and lymphomas, whose tissue initiator cells interact with the stroma creating a protective niche responsible for frequent relapse and drug resistance phenomena. To overcome these limitations, alternative approaches are emerging that rely on new biocompatible materials and modern technologies to fabricate three-dimensional (3D) structures able to simulate *in vitro* the complicated and intrinsically tridimensional microenvironment existing *in vivo*, thus supporting the comprehension of the causes and effects of cancer and the development of more effective therapies [6–11].

The present contribution proposes highly porous polymer scaffolds to mimic the bone marrow niche for blast cell culture. The scaf-

* Corresponding author.
Email address: antonella.sola@unimore.it (A. Sola)

https://doi.org/10.1016/j.msec.2018.10.086
Received 10 October 2017; Received in revised form 23 July 2018; Accepted 27 October 2018
Available online xxx
0928-4931/

Table 1
Experimental details for SCPL scaffolds. S1 stands for NaCl (Sigma-Aldrich), NHC for $NaHCO_3$ (Sigma-Aldrich), S2 for NaCl (Italkali, fine grained), and S3 for NaCl (Italkali, coarse grained).

Sample	Polymer matrix	Salt	Polymer-to-salt wt. ratio
Preliminary samples			
PMMA_S1_1:2	PMMA	S1	1:2
PMMA_NHC_1:2	PMMA	NHC	1:2
PMMA_S1 + NHC_1:2	PMMA	S1 + NHC (50/50)	1:2
PMMA_S1_1:3	PMMA	S1	1:3
PMMA_S2-NS_1:3	PMMA	S2-NS (S2, Not Sieved)	1:3
PMMA_S3-NS_1:3	PMMA	N3-NS (S3, Not Sieved)	1:3
Optimized samples			
PMMA_S2	PMMA	S2 (sieved)	1:4
PMMA_S3	PMMA	S3 (sieved)	1:4
PU_S2	PU	S2 (sieved)	1:4
PU_S3	PU	S3 (sieved)	1:4

folds were produced by means of the solvent casting particulate-leaching (SCPL) technique, that is currently very popular to fabricate polymer scaffolds for bone tissue engineering. In principle, the polymer is dissolved in an appropriate solvent and then an insoluble salt is admixed with the polymer solution. The solvent evaporation gives place to a salt-polymer composite, which is eventually washed to remove the salt particles. The SCPL method was chosen because it is relatively simple and straightforward, without the need for specific and expensive equipment; moreover, it allows to control the final porosity, pore size and interconnectivity by means of a proper selection of the polymer, of the porogen and of their relative amounts [12]. A recent development of the SCPL technique has demonstrated that, if the polymer solution is diffused in a steady salt stack and an appropriate thermal treatment is performed before leaching, even the crystallinity of the porous foam can be controlled closely [13]. However, in spite of its easiness and flexibility, so far the SCPL technique has been rarely applied to fabricate 3D supports for cancer research [14] and, to the best of the Authors' knowledge, this is the first time it is specifically exploited to reproduce the bone marrow microenvironment *ex vivo*. The present research encompasses therefore the development of finalized SCPL scaffolds, obtained from a rigid polymethyl methacrylate (PMMA) and from a flexible polyurethane (PU), and analyzes the effect of the fabrication conditions on the microstructure, on the mechanical behavior and on the mimicry of the final scaffolds. Nowadays other synthetic polymers, such as polycaprolactone (PCL) and poly(α-hydroxy acids), including PGA, PLA, and their copolymer PLGA, are most commonly used as scaffolding materials in tissue engineering on account of their biodegradability. In fact, they are designed on purpose to degrade *in-vivo* and to be replaced gradually by the healing bone tissue [15,16]. However, in the present context non-biodegradable polymers should be applied instead, because they are expected to remain unchanged upon cell culturing and therapy assessment. Preference was given to PMMA and PU due to their promising potentialities. Even if it is conventionally used as self-hardening cement for orthopedic implant fixation rather than as scaffolding material in bone tissue engineering, PMMA is an interesting candidate for the production of substrates for cell culturing on account of its good biocompatibility characteristics (solid PMMA is an FDA approved implant material) and relatively high elastic modulus up to approximately 2 GPa [17].

Polyurethanes have a segmented molecular structure including di- or poly-isocyanates (hard segments) and di- or poly-ols (soft segments), which makes it possible to control their physical and mechanical properties on a wide range, depending on the composition

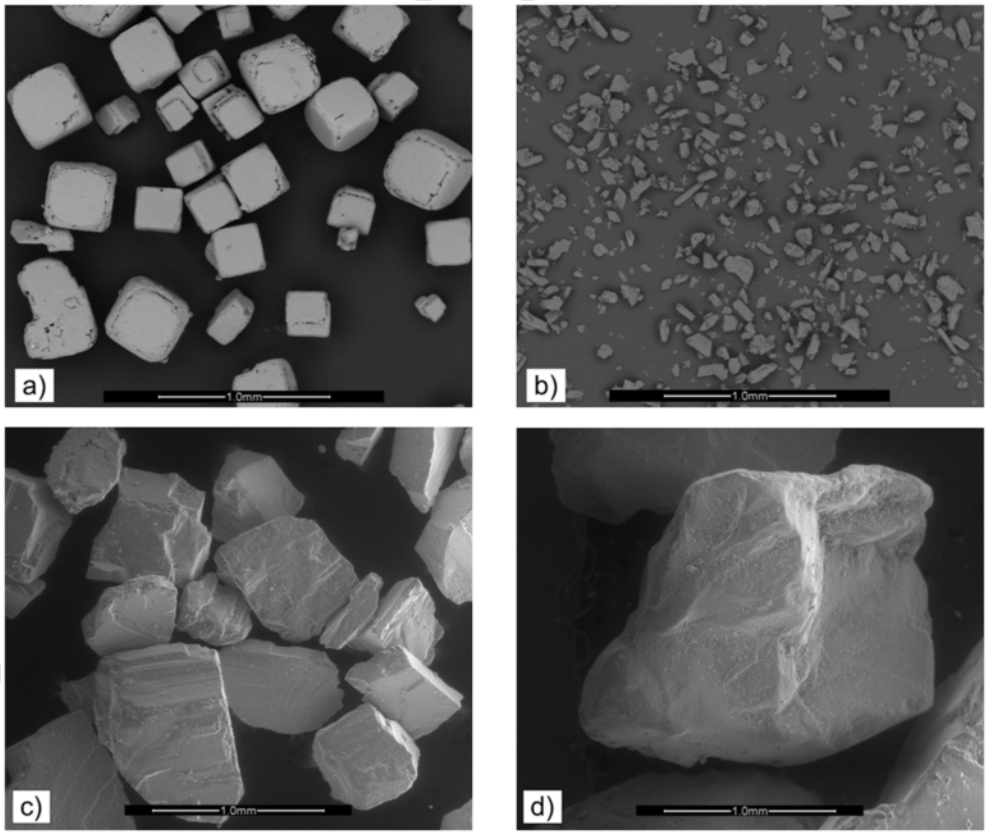

Fig. 1. Salt particles: S1 (a), NHC (b), S2 after sieving (c) and S3 after sieving (d). Scale bar: 1 mm.

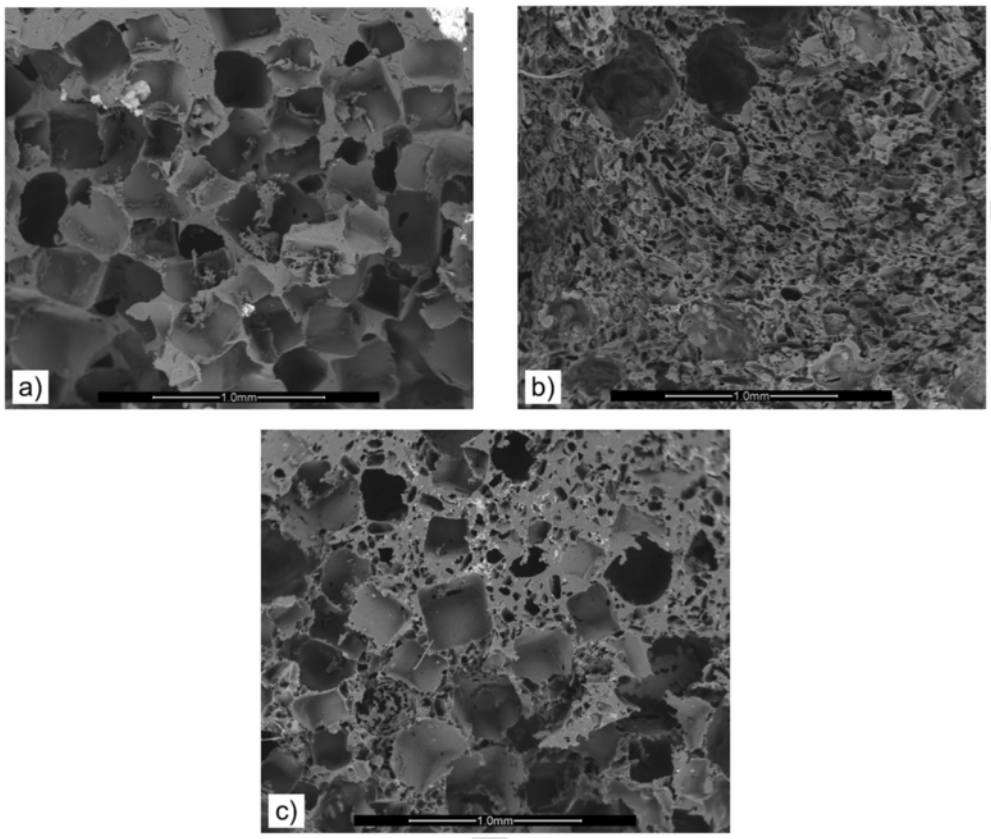

Fig. 2. Pilot SCPL scaffolds in PMMA: PMMA_S1_1:2 (a), PMMA_NHC_1:2 (b), and PMMA_S1 + NHC_1:2 (c). Scale bar: 1 mm.

and the synthesis procedure that is applied. They are characterized by biocompatibility and moderate compatibility with blood and, though originally addressed to artificial skin, vascular grafts, neural connections, and articular cartilage reconstruction applications, they are now emerging also as suitable scaffolding materials [18,19].

2. Materials and methods

2.1. Preparation of SCPL scaffolds

Two different polymers were compared for the matrix, namely poly(methyl methacrylate), "PMMA" (Optix CA-1000 I, Optix Acrylic Resins, Plaskolite Inc. Columbus, Ohio, U.S.A.; properties available on-line [20]), and polyurethane, "PU" (Z1A1, Biomer Technology Ltd., Cheshire, England; properties available on-line [21]). Both polymers were used as received, without any purification prior to scaffold fabrication.

The research included the production of preliminary samples, to determine the effect of the processing conditions, and the fabrication and subsequent characterization of the optimized scaffolds. PMMA was the matrix for all the preliminary samples, which were produced and analyzed to assess the role of the salt type, of the salt particle size and of the polymer-to-salt ratio. In order to create the porosity, various salts were compared, including NaCl, hereafter "S1" (Sigma-Aldrich, CAS number 7614-14-5), $NaHCO_3$, "NHC" (Sigma-Aldrich, CAS number 144-55-8), as well as fine-grained and coarse-grained marine NaCl for dietary use (Italkali Società Italiana Sali Alcalini S.p.A.). For the preliminary samples, the marine NaCl salts were used as received, without sieving (for these "not sieved" salts, the labels "S2-NS" and "S3-NS" were used to indicate the fine-grained powder and the coarse-grained one, respectively); for the optimized samples, instead, the fine-grained salt was sieved below 1000 μm (= 1 mm), whereas the coarse-grained salt was sieved between 1000 μm (= 1 mm) and 2000 μm (= 2 mm); for these sieved salts, the names "S2" and "S3" were adopted for simplicity.

Tetrahydrofuran, "THF" (Analar Normapur (VWR), CAS 109-99-9), was employed to dissolve the PMMA granules, whereas a 50-50 mixture of *N*,*N*-dimethylformamide, "DMF" (Sigma, CAS Number 68-12-2), and of THF was used for PU.

In the general procedure, the polymer was dissolved in the appropriate medium (PMMA in THF, typical concentration: 20 g PMMA/100 ml THF; PU in DMF + THF, typical concentration: 12 g PU/100 ml DMF + THF); the salt was added to the polymer solution according to a prefixed polymer-to-salt ratio and stirred until uniformly dispersed; the dispersion was poured into silicon moulds. The solvent was left to evaporate overnight, then the samples were extracted from the moulds and generously rinsed with distilled water, to start removing the salt. The samples were soaked in distilled water for a week, replacing the water twice a day; to conclude they were sonicated in distilled water for 30 min and left to dry in ambient conditions. Table 1 lists all the samples with the corresponding experimental details.

2.2. Characterization

The salt particles for SCPL as well as the scaffolds were observed with an environmental scanning electron microscope, "ESEM" (FEI Quanta, The Netherlands), operated in high vacuum mode, for the salts, or in low vacuum mode, for the scaffolds (0.68 bar).

The granulometric size distribution of the salt particles used for the optimized SCPL scaffolds (namely S2 and S3 sieved marine salts) was determined with a laser granulometer (Mastersizer 2000 Ver. 5.22, Malvern Instruments Ltd., Malvern, UK); the salts were dispersed in ethanol (Baker, CAS number: 64-17-5).

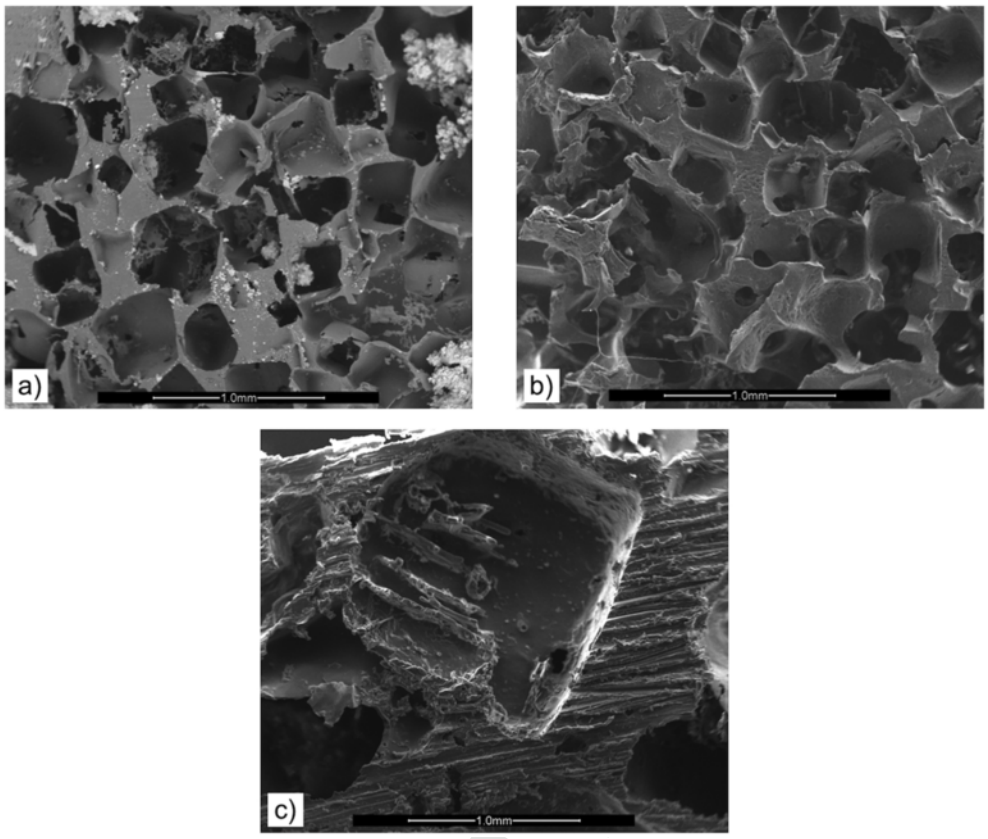

Fig. 3. Pilot SCPL scaffolds in PMMA: PMMA_S1_1:3 (a), PMMA_S2-NS_1:3 (b), and PMMA_S3-NS_1:3 (c). Scale bar: 1 mm.

The Fourier transform infrared spectroscopy, "FT-IR" (FTIR VERTEX 70), was carried out on the original polymers, as well as on the scaffolds, working under the attenuated total reflection (ATR) mode, in the 4000 cm^{-1}–600 cm^{-1} range. Each spectrum was the average over 30 scans.

The X-ray diffraction ("XRD", X'pert PRO, PANalytical, Almelo, The Netherlands) was performed on 10 mm × 10 mm × 3 mm scaffolds by using the CuKα radiation (λ = 1.54 Å); the scans were acquired in the 10°–90° 2θ range, with a step size of 0.008° 2θ and a scan step time of 30.48 s.

The porosity P was estimated by measuring the volume, v_{sc}, and the mass, m_{sc}, of the scaffolds (at least 5 samples for each type) and then applying the formula:

$$P = \left(1 - \frac{m_{sc}}{\rho_p v_{sc}}\right) \quad (1)$$

where ρ_p is the polymer density (1.16 g/cm^3 for PMMA [20] and 1.10 g/cm^3 for PU [21]).

The scaffolds were cut manually to a dimension of 8 mm × 8 mm × 3 mm. Then, compressive tests were performed at room temperature on a TA DMA Q800 (TA Instruments, New Castle, DE, USA) equipped with an 18 N load cell; the applied load was increased at a constant rate of 1 N/min. For each sample, the force and deflection data acquired by the instrument were converted to engineering stress and strain values, respectively, and the compressive Young's modulus, E, was calculated as the slope of the stress-strain curve according to the equation

$$E = \frac{\sigma_2 - \sigma_1}{\varepsilon_2 - \varepsilon_1} \quad (2)$$

where ε_2 and ε_1 are the strain values at two selected points of the stress-strain curve and σ_2 and σ_1 are the corresponding stresses. For each polymer matrix, appropriate portions were considered on the stress-strain curve in order to analyze the linear elastic behavior. All the values for E were calculated as means of five measurements (± standard deviation).

The stability of the scaffolds was tested in common sterilizing media. Since PMMA is expected to be soluble in ethanol-water solutions [22], pure ethanol was considered for PMMA-based scaffolds, whereas a 75% ethanol solution was used for PU-based scaffolds. The scaffolds were immersed for 4 days and the soaking liquid was refreshed once a day. A standard volume of 50 ml was used for 5 mm × 5 mm × 3 mm scaffolds. After soaking, the scaffolds were left to dry in ambient conditions, gently rinsed with distilled water and left to dry in ambient conditions again. The effect of soaking was assessed *via* ESEM observation and FT-IR analysis.

2.3. Cell culture and viability tests

PMMA and PU supports were sterilized by immersion in 10 ml of 100% ethanol or 75% ethanol, respectively, for 24 h in a mixing rotator. They were then washed for 24 h with sterile water to get rid of ethanol. No contamination was detected over the culture period in all samples tested.

The supports were glued to the bottom of a 12-well plate using 5 μL of THF, and coated with the extracellular matrix component type IV collagen (Sigma-Aldrich) at a dilution of 150 μg/ml in Dulbecco's Phosphate Buffered Saline (PBS), for 2 h at room temperature on a shaker. Wells were then filled with RPMI 1640 culture medium additioned of 10% FBS, 100 U/ml Penicillin/Streptomycin, 100 U/l L-Glutamine (Euroclone), to soak PU and PMMA supports, and left sit for 24 h at 37 °C with 5% CO_2.

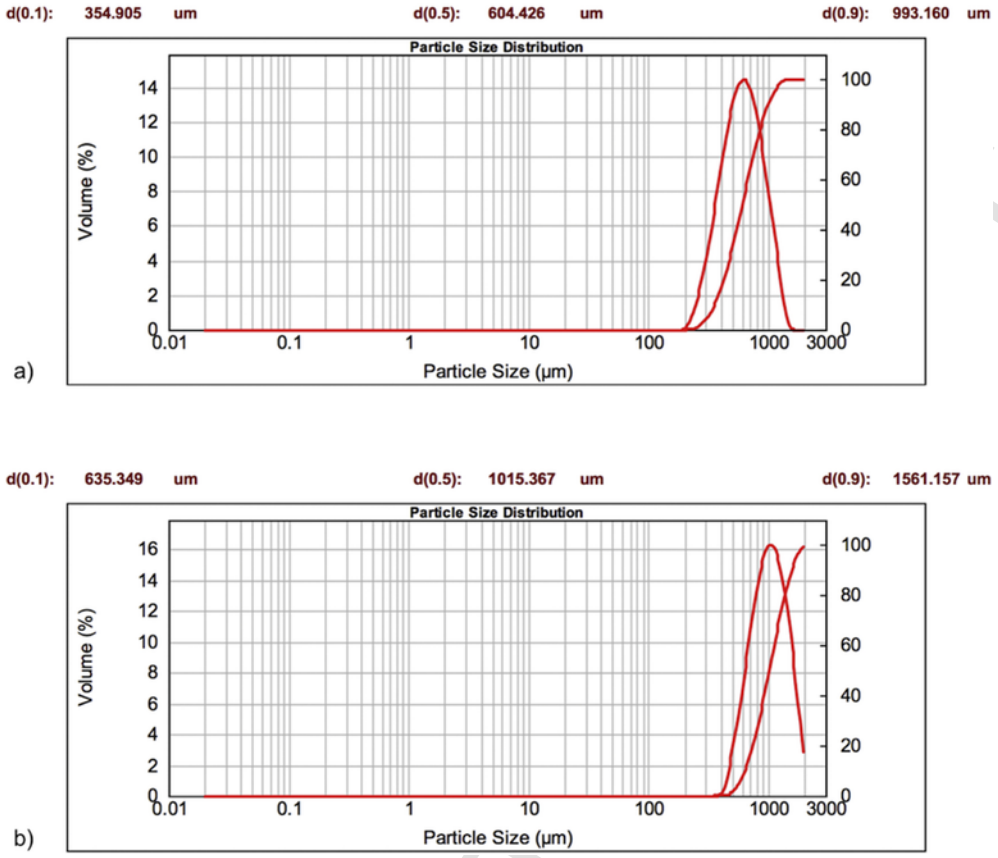

Fig. 4. Granulometric curves of the salts used to process the optimized scaffolds: S2 sieved below 1000 µm (a) and S3 sieved between 1000 µm and 2000 µm (b).

Collagen-coated scaffolds (5 mm × 5 mm × 5 mm cubes) were observed with a Nikon SMZ7457 stereomicroscope (Nikon Instruments Europe B.V., Italy) to verify the porous architecture after coating.

For immunofluorescence analysis, collagen-coated scaffolds, seeded with 1×10^5 HS5 cells, after 16 h were fixed for 15 min with 4% paraformaldehyde, and then stained with DAPI and Cy3-phallodin 1:100 [Millipore]. Confocal imaging was performed by a Nikon A1 confocal laser scanning microscope (Nikon Instruments Europe B.V., Italy), and three-dimensional pictures of scaffold surfaces were obtained by 50 Z series (3 µm each), in order to reach around 150 µm depth.

The scaffolds were centrally cut and the inner core analyzed. The confocal serial sections (20 Z series, 1 µm each) were processed with ImageJ software to obtain three-dimensional projections. The image rendering was performed by Adobe Photoshop software.

Jurkat cells, a T-acute lymphoblastic leukemia cell line, were grown in suspension in full RPMI 1640. Human Stromal-5 (HS-5) cells were seeded on top of the scaffolds at a density of 1×10^5 cells/well and allowed to enter inside the pores for 24 h. In co-culture experiments, Jurkat cells were added to the HS5-containing wells after 24 h at a density of 4×10^5 cells/well [23]. Cell adhesion to the supports was tested by fixation in 4% paraformaldehyde for 15 min at room temperature and nuclear staining with the DNA binding fluorescent stain 4′,6-diamidino-2-phenylindole (DAPI) for 15 min at room temperature, and observation with an inverted Nikon A1 confocal laser scanning microscope [24,25]. For cytotoxicity experiments, 24 h after seeding, cells were additioned with the dual PI3K and mTOR inhibitor PF-04691502 or with DMSO vehicle. Cytotoxicity was assessed both by MTT (Sigma-Aldrich) and Annexin V analysis. Briefly, 24 h after treatment co-cultured cells were trypsinized, washed in PBS and incubated with 4 µl of phycoerythrin (PE)-conjugated anti-CD5 monoclonal antibody (BD) for 20 min at room temperature in the dark, to selectively stain Jurkat cells. To detect apoptosis, samples were incubated with Annexin V–FITC (Sigma Aldrich) in binding buffer (10 mM HEPES pH 7.4, 140 mM NaOH, 2.5 mM CaCl2) for 15 min at room temperature in the dark. Moreover, cells from single cultures were collected, washed with PBS and stained with Annexin V–FITC in Annexin V binding buffer for 15 min at room temperature in the dark. All samples were then analyzed by flow cytometry with a Coulter Epics XL MCL equipment. Annexin V positive (Annexin V^+) cells are apoptotic cells.

3. Results and discussion

3.1. Preliminary scaffolds: effect of salt type

In order to investigate the effect of the salt type, three pilot samples were produced with S1 (scaffold PMMA_S1_1:2), with NHC (scaffold PMMA_NHC_1:2), and with a 50-50 mixture of S1 and NHC salts (scaffold PMMA_S1 + NHC_1:2); to fix the attention on the porogen, PMMA was consistently used as the matrix and the polymer-to-salt ratio was fixed to 1:2. As shown in Fig. 1, it should be underlined that the two salt powders used for these preliminary scaffolds, namely S1 and NHC, differ not only in chemical composition, but also in grain size and morphology. The S1 particles are indeed cubic (Fig. 1a), whereas the NHC ones are more irregular and often elongated (Fig. 1b); analogously, the S1 particles are larger than the NHC counterparts. For comparison, Fig. 1 also includes the micrographs of the sieved S2 and S3 salts used for the optimized scaffolds.

Since the pores of SCPL scaffolds are the cavities left by the salt particle removal, the pores in PMMA_S1_1:2 basically preserve a cubic geometry (Fig. 2a), whilst the pores in PMMA_NHC_1:2 are finer

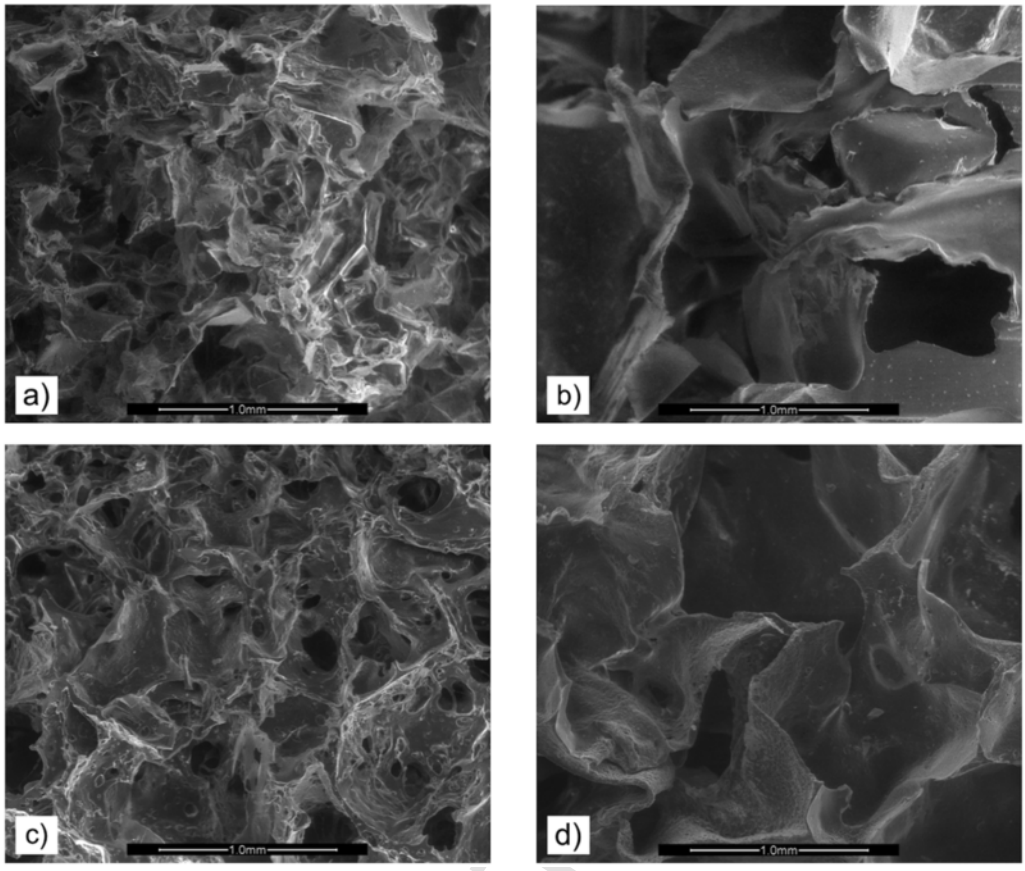

Fig. 5. Microstructure of the optimized scaffolds: PMMA_S2 (a), PMMA_S3 (b), PU_S2 (c), and PU_S3 (d). Scale bar: 1 mm.

Table 2
Porosity (mean value ± standard deviation) estimated through Eq. (2) and compressive modulus at appropriate strain intervals/values for PMMA_based scaffolds and for PU_based ones.

Scaffold	Porosity [%]	Compressive modulus, E_c [kPa]		
PMMA scaffolds		Strain: 0.3–0.7%		
PMMA_S2	84.3 ± 1.5	1283 ± 803		
PMMA_S3	87.4 ± 3.3	1143 ± 675		
PU scaffolds		Strain: 0.3–0.7%	Strain: 40%	Strain: 70%
PU_S2	91.3 ± 0.9	29 ± 9	50 ± 6	493 ± 76
PU_S3	82.1 ± 2.3	75 ± 27	150 ± 44	1883 ± 181

and more irregular (Fig. 2b). Obviously, PMMA_S1 + NHC_1:2 exhibits both types of pores (Fig. 2c). The pores in PMMA_S1_1:2 create a continuous network; the porosity is rich and open, but not perfectly even throughout the cross section, probably as a consequence of the partial precipitation of salt during processing. To the contrary, if NHC is used, the porosity, though rich, is less obviously continuous. Most of all, the pores induced by NHC are much smaller. The pore size in scaffolds for cell culturing plays a key role, because pores must be large enough to support efficient diffusion of nutrients and oxygen for cells; a diameter of at least 100 μm is strictly required to the purpose [26]. This pre-requisite substantially does not permit the use of NHC, since the obtained pores are too small. However, in view of the addition of the collagen coating, which is expected to reduce the usable pore size, also the pores left by S1 particles may be too small, since the average edge length of the salt grains, which determines the pore size, is about 260 μm.

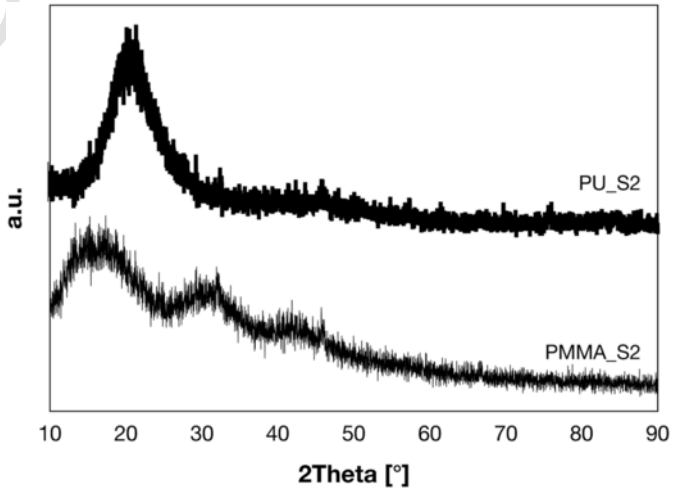

Fig. 6. XRD spectra acquired on PMMA (thin line) and PU (bolt line) scaffolds (with salt S2).

3.2. Preliminary scaffolds: effect of polymer-to-salt ratio

In order to enrich the porosity and homogenize its distribution, the polymer-to-salt ratio was modified from 1:2 to 1:3; additionally, the S1 salt was substituted with two common salts whose grain size was larger. As previously anticipated, for these pilot samples, the new S2 and S3 salts were used as received, without sieving. Fig. 3 compares the three pilot PMMA scaffolds obtained with S1, S2-NS and S3-NS and with a polymer-to-salt ratio of 1:3.

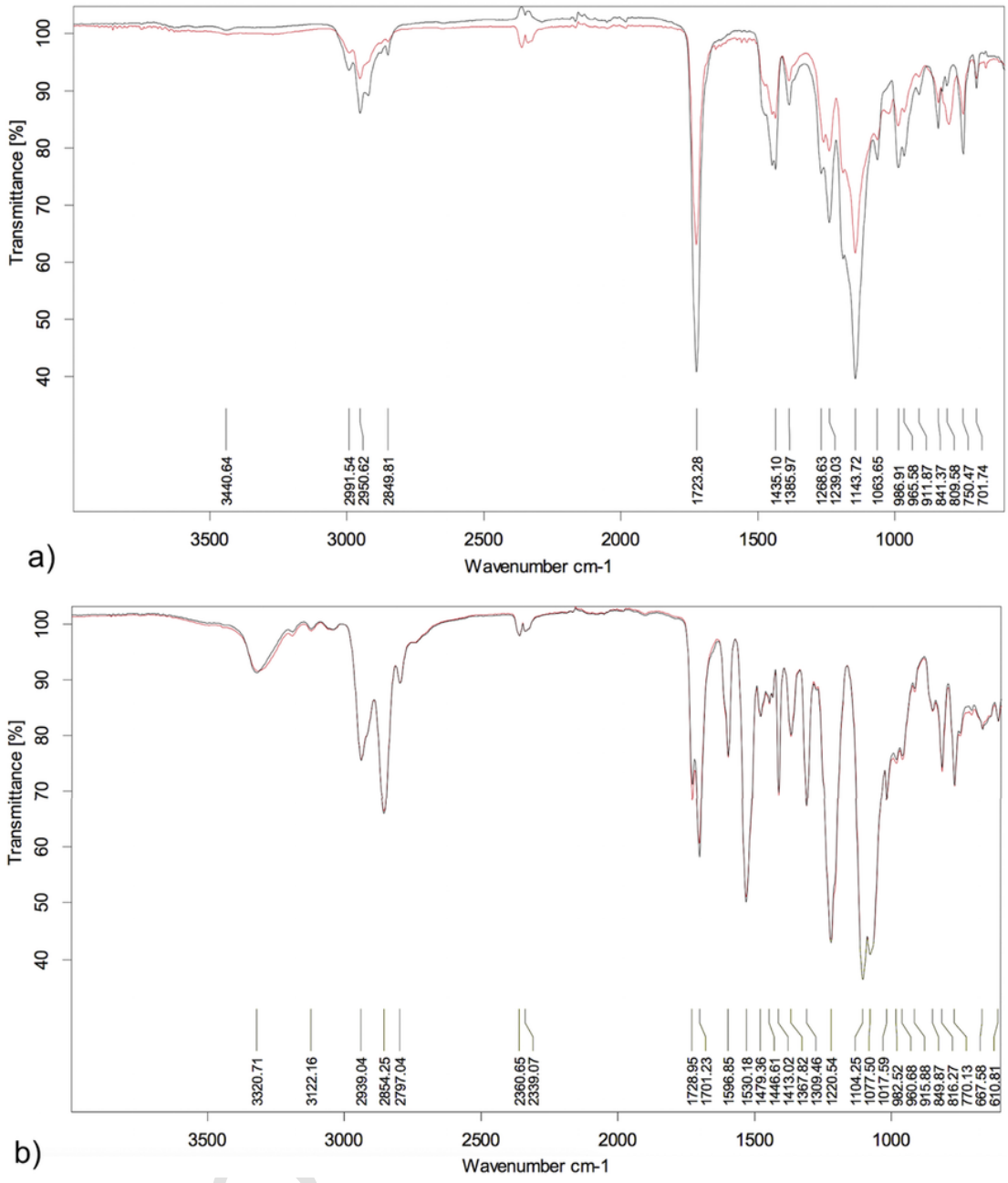

Fig. 7. FT-IR analysis performed on PMMA (a) and on PU (b) systems. In both graphs, black line: original polymer pellet; red line: corresponding scaffold (with salt S2). (For interpretation of the references to colour in this figure legend, the reader is referred to the web version of this article.)

The increase in the relative amount of porogen gives place to a richer porosity (sample PMMA_S1_1:3, Fig. 3a); however, the polymer struts are still relatively thick, thus suggesting the possibility of modifying the polymer-to-salt ratio further, namely from 1:3 to 1:4. Though not sieved, the new salts, S2-NS (sample PMMA_S2-NS_1:3, Fig. 3b) and S3-NS (sample PMMA_S3-NS_1:3, Fig. 3c), are able to imprint larger pores and they are therefore preferable to S1.

3.3. Optimized scaffolds

3.3.1. Microstructure

On account of the previous results, the final scaffolds were manufactured with a polymer-to-salt ratio of 1:4. Moreover, in order to control the pore size more closely, the fine-grained and coarse-grained salts were sieved into two complementary grain size ranges, namely below 1000 μm (salt "S2") and between 1000 and 2000 μm (salt "S3"). The corresponding granulometric curves, which are reported in Fig. 4, are mono-modal for both powders, with d(0.5) = 604 μm for S2 and d(0.5) = 1015 μm for S3.

In this way, highly porous and well interconnected sponge-like structures could be achieved both with PMMA and with PU, as shown in Fig. 5. Regardless of the polymer matrix, the porogen concentration was indeed high enough to create a well interconnected network thanks to close geometric packing [27], whereas increasing further the relative amount of porogen brought about a loss of structural continuity (data not shown) since the polymer was not enough to fill the space between the salt particles, which impeded the complete development of the polymer struts [28]. The improved interconnectivity with respect to the preliminary samples also depends on the shape of the S2 and S3 salt particles [27], that is still irregular

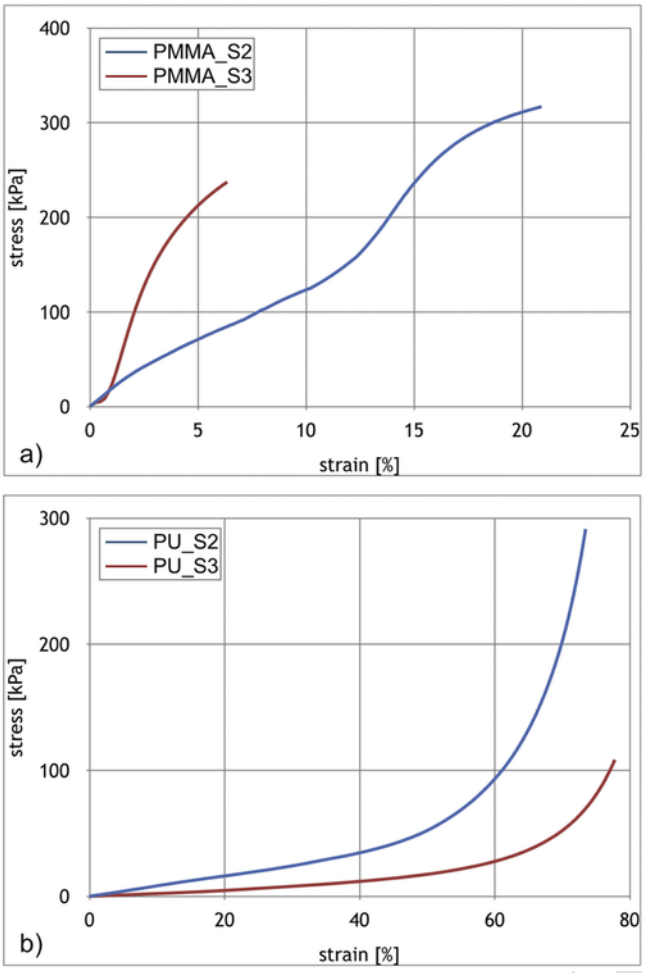

Fig. 8. Stress-strain compressive curves for PMMA-based scaffolds (a) and PU-based ones (b).

but more spherical with respect to the strictly cubic geometry of S1, as shown in Fig. 1.

At higher magnification, the PU-based scaffolds exhibit a fine microporosity and surface roughness, which presumably originate from the use of DMF and THF to dissolve the polymer. In fact, according to the contribution by Gorna and Gogolewski [29], DMF works as solvent, whereas THF works as non-solvent. The difference in their solubility parameters causes a liquid-induced phase separation that results in the formation of micropores, especially on the walls of the macro-pores left by the salt particles [29]. As previously mentioned in the Experimental section, the surface of the present scaffolds has to be coated with collagen, in order to improve the affinity of the polymer substrate with cells [28,30]. However the intrinsic microporosity and fine irregularity of the PU struts may play an advantageous role, since it is known from the literature that the surface roughness of scaffolds enhances attachment, proliferation and differentiation of cells [31].

With a focus on the macro-pores left by the salt particles, an attempt was made to elaborate the SEM images to measure the porosity and the mean pore size of the scaffolds. Nevertheless, the porosity of the S2-derived scaffolds is too fine and complicated to allow a reliable calculation; also for the S3-derived scaffolds, the intrinsic tridimensionality of the cellular architecture limits the significance of the image elaboration. In spite of this hindrance, as a demonstration the image elaboration was completed on the PU_S3 scaffolds, which possess a mean pore size of 1.12 mm (expressed as mean equivalent diameter) and an average porosity of 92%. The mean pore size matches very well the value of d(0.5) = 1015 μm obtained for the S3 powder (Fig. 4b).

As an alternative approach, the porosity was calculated from the mass and volume of the scaffolds. The results are listed in Table 2.

For PMMA-based scaffolds, the mean porosity is similar for both porogens, whereas the mean porosity of PU_S2 is sensibly higher than that of PU_S3. This is in agreement with the trends observed by Sin et al., who investigated PU-based scaffolds produced by SCPL with and without an additional centrifugal step [28].

3.3.2. X-ray diffraction

The XRD spectra acquired on the scaffolds should be considered with caution, since the optimal geometric conditions for diffraction were not respected in every single point of the nominal surface of the samples due to the complicated three-dimensional architecture of cellular materials. However, as exemplified in Fig. 6, the polymer matrix was substantially amorphous both in PMMA- and PU-based scaffolds, which is coherent with the limited tendency to crystallize of porous systems with respected to bulk counterparts that has been recently reported in the literature for PLA-based SCPL scaffolds [13]. No peaks could be attributed to the residual presence of porogen (NaCl), thus confirming the achievement of a well interconnected and open porosity and, at the same time, the effectiveness of the wash-out step. Analogous diffractograms were collected both for S2 and S3 salts (data not shown).

3.3.3. Infrared spectroscopy

In order to check the possible effects of processing on the polymer structure, the FT-IR analysis was performed on the original polymer pellets, to define a benchmark (black lines in Fig. 7), and on the corresponding scaffolds (red lines). For clarity reasons, Fig. 7 proposes the spectra acquired on the scaffolds processed with the S2 particles, but those with S3 are equivalent. For PMMA, the trend is qualitatively the same for the original polymer and for the scaffold, even if the peaks are more intense and defined for the former than for the latter. The differences are more detectable in the fingerprint range between 987 cm^{-1} and 810 cm^{-1}. The attribution of the single peaks in this area is not straightforward, but the band at 962 cm^{-1} can be assigned to the C—CH_3 bending [32], which is likely to be affected by the solvent action during processing. To the contrary, the PU spectra are identical before and after processing, thus proving that the polymer structure was not altered by the manufacturing process.

3.3.4. Mechanical properties

Even if the present scaffolds are not intended for load bearing, their mechanical properties are relevant, because the scaffolds must be easy to handle. Moreover, it is known from the literature that, in principle, the stiffness of a scaffold influences inter-/intracellular signaling, cell growth and motility, and response to stimulation or inhibition [3].

Representative stress-strain graphs are reported in Fig. 8a, for PMMA-based scaffolds, and in Fig. 8b, for PU-based ones. Since PMMA is a relatively stiff polymer (tensile modulus E_p: 295000 psi ≈ 2034.0 MPa [20]) whereas PU is a relatively flexible one (tensile modulus (at 50% strain) E_p: 3.1 MPa [21]), also the compressive behavior of the corresponding scaffolds is sensibly different and therefore the stress-strain graphs are not directly superimposing; in more detail, being the stress the same (up to about 300 kPa), the strains achieved during testing are much higher for the PU-based scaffolds than for the PMMA-based ones.

Generally speaking, if the PMMA-based scaffolds are considered, the stress-strain graphs of the PMMA_S2 samples have a first, short linear segment, followed by a second, steeper segment for strains ex-

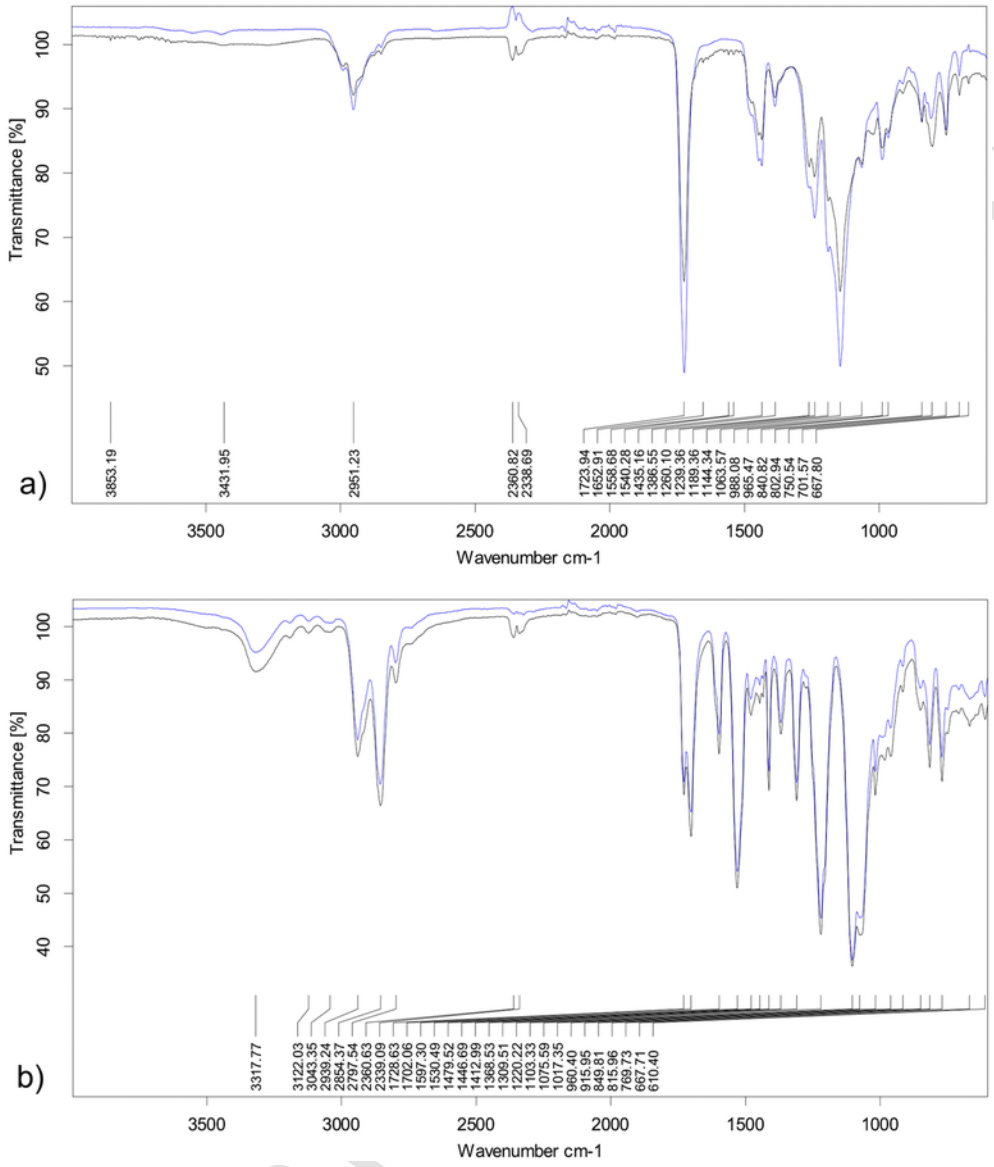

Fig. 9. FT-IR analysis performed on PMMA (a) and on PU (b) scaffolds to assess the effect of sterilizing media. In both graphs, black line: original scaffold; blue line: scaffold soaked in sterilizing medium for 4 days (scaffolds produced with salt S2). (For interpretation of the references to colour in this figure legend, the reader is referred to the web version of this article.)

ceeding 1%. Even if the slope of the stress-strain curves for the PMMA_S3 scaffolds is almost constant over a wider range, up to a strain of about 10%, for comparison E_c was calculated in the 0.3–0.7% strain interval for all the PMMA-based scaffolds.

The compressive behavior of the PU-based scaffolds remains substantially linear up to a strain of 30%, then the slope of the stress-strain curve progressively increases, especially for the PU_S2 scaffolds; being the strain the same, the stress is indeed systematically higher for the PU_S2 scaffolds than for the PU_S3 ones. On account of the high deformability of the PU-based scaffolds, E_c was calculated over the 0.3–0.7% strain interval in order to have a term of comparison with the PMMA-based scaffolds, but it was also calculated at 40% and at 70% of strain (for the latter two values, E_c was determined as the tangent slope).

All the results for E_c calculations are summarized in Table 2. If the values in Table 2 are considered, it is apparent that, coherently with the superior stiffness of PMMA with respect to PU, E_c in the 0.3–0.7% strain interval is higher for the PMMA-based scaffolds than for the PU counterparts. The high standard deviation signifies that the data in Table 2 are spread over a wide range, however E_c is, on average, higher for the PMMA_S2 scaffolds than for the PMMA_S3 ones. This is likely due to the different porosity, that is indeed lower for the PMMA_S2 scaffolds than for the PMMA_S3 ones, as previously seen in the same Table 2. Analogously, if the PU-based scaffolds are compared, E_c is relevantly higher for the PU_S3 scaffolds than for the PU_S2 ones, again as a result of the difference in porosity observed for these scaffolds. A similar result has already been reported in the literature for PU-based SCPL scaffolds designed for cardiac tissue engineering [28].

From the graphs in Fig. 8 as well as from the results in Table 2, it is clear that the values calculated for E_c are influenced by the applied load, on the one hand, and by the scaffold's features, especially the polymer type and the porosity, on the other. Independently of the specific scaffold type, E_c depends indeed on the applied load and consequent strain, with a trend that implies at first a plateau and then a progressive rise, that becomes very steep for high strain values. As a matter of fact, the initial elastic deformation of the struts is followed by subsequent folding, which causes the scaffold to pack

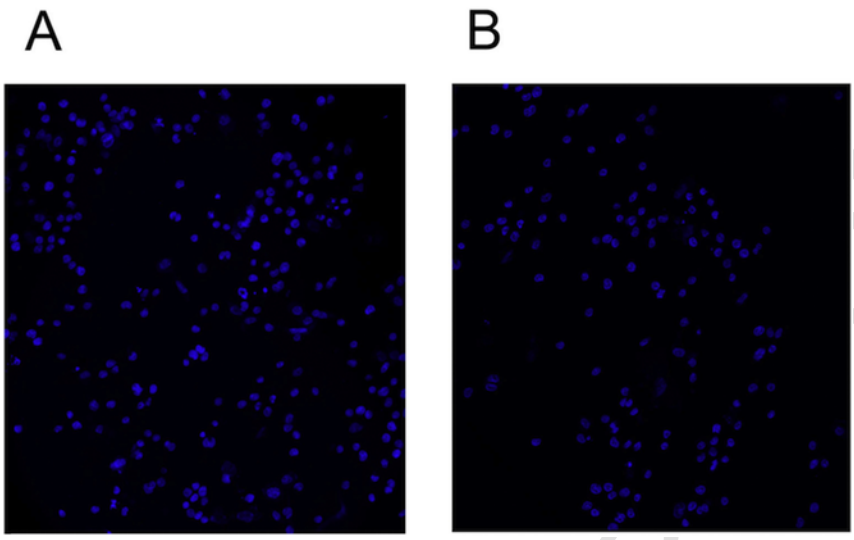

Fig. 10. HS-5 cells were grown associated to collagen-coated composites. DAPI staining of cells seeded on PU (left panel) or PMMA (right panel) 3D-supports indicates that cell nuclei have a normal and regular shape, characteristic of healthy cells. A representative image of each support is shown. Overlapping results were obtained for both pore sizes.

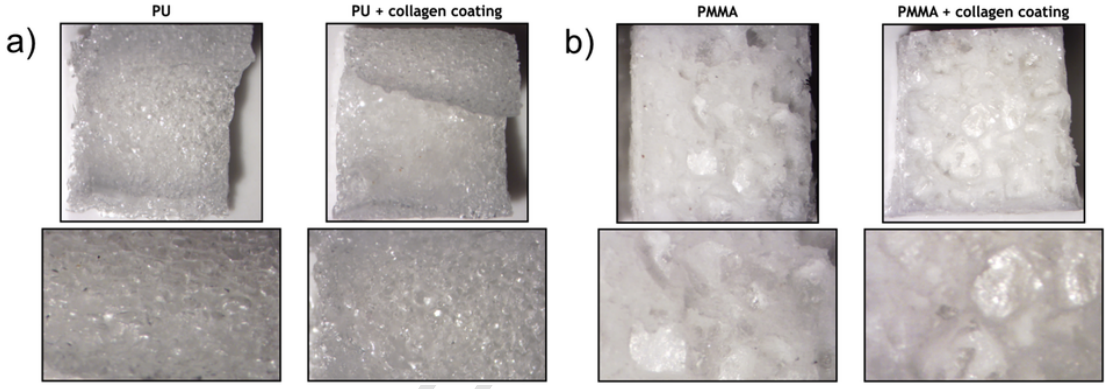

Fig. 11. Porous architecture before and after collagen coating. (a) PU_S2 scaffold; (b) PMMA_ S3 scaffold. Tested samples: 5 mm × 5 mm × 5 mm cubes. Low magnification images: standard zoom 0.67; high magnification images: standard zoom 1.

and behave like a "massive" (*i.e.* not porous) bulk material, with a resulting increase in E_c [28].

If the effect of the polymer type and of the porosity is considered, according to the models proposed by Gibson and Ashby [33] to describe the linear elastic behavior of three-dimensional cellular materials under compression, the compressive modulus E_{sc} of an open-cell scaffold should depend on the Young's modulus of the polymer struts, E_p, and on the relative density $??_{sc}/??_p$ as:

$$\frac{E_{sc}}{E_p} = C\left(\frac{\rho_{sc}}{\rho_p}\right)^2 \tag{3}$$

where C is a constant whose value is usually assumed to be 1 [33]. For the present scaffolds, $??_p$ is 1.16 g/cm^3 for PMMA [20] and 1.10 g/cm^3 for PU [21], whereas the densities of the corresponding scaffolds $??_{sc}$ are directly associated to the porosity values listed in Table 2. The previsional compressive modulus should be therefore 50,070 kPa for PMMA_S2, 32,664 kPa for PMMA_S3, 24 kPa for PU_S2 and 99 kPa for PU_S3. If compared to the results in Table 2, the obtained values are in good agreement with the experimental ones for PU-based scaffolds, but not for PMMA-based ones.

Jo et al. [34] proposed specific models to describe the compressive behavior of PMMA open-cell foams and they calculated the compressive modulus as:

$$\frac{E_{sc}}{E_p} = C_0\left[C_1\left(\frac{\rho_{sc}}{\rho_p}\right)^4 + C_2\left(\frac{\rho_{sc}}{\rho_p}\right)^3 + C_3\left(\frac{\rho_{sc}}{\rho_p}\right)^2 + C_4\left(\frac{\rho_{sc}}{\rho_p}\right)^1 + C_5\right] \tag{4}$$

where $C_1 = 0.2515$, $C_2 = 0.2073$, $C_3 = 0.06409$, $C_4 = 0.008801$, and $C_5 = 0.0004533$ [34]. For PMMA open-cell foams, the constant C_0 was experimentally determined to be 1.88 [34]. Strictly speaking, Eq. (4) should be applied for $0.2 < ??_{sc}/??_p < 0.8$, whereas $??_{sc}/??_p$ is here about 0.157 for PMMA_S2 and 0.127 for PMMA_S3, which means that the present scaffolds are slightly more porous than the typical cellular materials encompassed by the model of Eq. (4). However, as an indication, the previsional compressive modulus E_{sc} calculated according to Eq. (4) should be 16,690 kPa for PMMA_S2 and 11,795 kPa for PMMA_S3. Again, the calculated values overestimate the real ones.

Since the predicted values for PMMA scaffolds deviate from the experimental data for both models, it is plausible that the problem derives from the input data. In fact, the analytical results are strongly affected by the value of E_p used to calculate them. As a first approximation, the (tensile) elastic modulus of the pristine polymer was introduced for E_p both in Eq. (3) and in Eq. (4). However, as remarked by Gibson and Ashby [33], the real value of the elastic modulus of the scaffold matrix is rarely known with precision, as it depends on

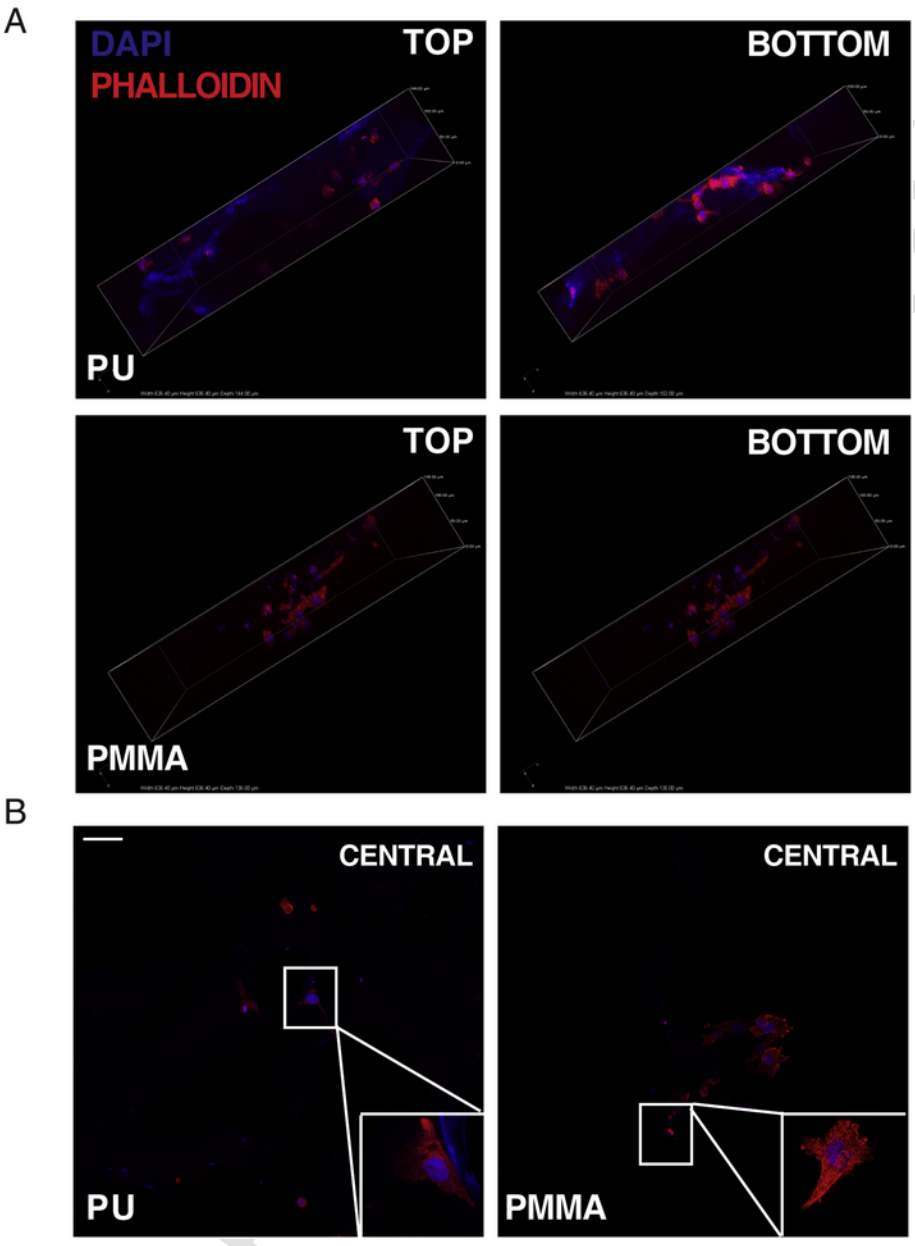

Fig. 12. Scaffold colonization by HS5 cells. PU and PMMA scaffolds, seeded with HS5 cells, were treated for immunofluorescence analysis. DAPI and Cy3-phallodin staining reveals the nuclei in blue and the actin cytoskeleton in red, respectively. A) Representative three-dimensional pictures of 150 μm depth of TOP and BOTTOM sides of PU and PMMA scaffolds show the cell distribution under the scaffold surfaces. B) Representative three-dimensional projections of the middle part (CENTRAL) are shown for both the scaffolds. Scale bar = 20 μm for all images. Triple magnification of one cell is shown in white squares to monitor cell morphology. (For interpretation of the references to colour in this figure legend, the reader is referred to the web version of this article.)

the degree of polymer-chain alignment, on chemical changes brought about by the fabrication process, on the possible aging and/or oxidation of the polymer and other uncontrolled phenomena [33]. For the PMMA-based scaffolds considered here, it is likely that some changes occurred during processing as supported by the FT-IR analysis, thus modifying the elastic modulus of the scaffold's matrix with respect to the unprocessed polymer. Nonetheless, it is worth noting that, as expected, the PMMA-based scaffolds are sensibly stiffer than the PU-based ones. Additionally, all the produced scaffolds can be easily handled without neither breaking nor collapsing.

3.3.5. Stability in sterilizing media

Before seeding with cells, the scaffolds must be sterilized by immersing them in an appropriate liquid and then exposing them to UV light. In order to test their chemical stability, both PMMA-based scaffolds and PU-based ones were conditioned in pure ethanol and in 75% ethanol for four days, respectively. The prolonged soaking time, which was obviously longer than the real one (that is typically in the order of minutes), was addressed to amplify the effect of the sterilizing medium. According to the ESEM observation, the original porous architecture was not altered in any of the analyzed scaffolds (data not reported). FT-IR spectra were also acquired on the scaffolds to investigate more closely the effect of the sterilizing media on the polymer structure. As a term of comparison, Fig. 9 shows the overlays of the spectra acquired on the pristine (not-soaked) scaffolds and those acquired after soaking. For the sake of brevity, Fig. 9 includes the spectra acquired on the scaffolds produced with the S2 particles only, but those with S3 are analogous. Since no significative changes

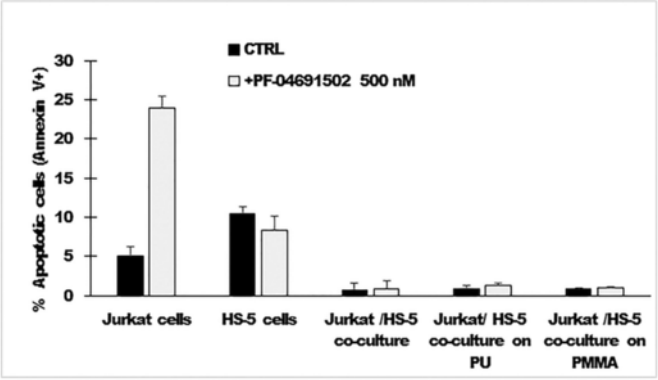

Fig. 13. The apoptotic Jurkat cells sub-population was identified by dual staining with an anti-CD5+ antibody to detect Jurkat cells, together with Annexin V to detect apoptosis, as described in Materials and Methods. Overlapping results were obtained for both pore sizes.

were detected in the respective spectra, pre- and post-immersion, even after soaking for 4 days, it is reasonable to conclude that the immersion in sterilizing media is not modifying the structure of the polymer matrices, provided that pure ethanol is used for PMMA-based scaffolds and 75% ethanol is used instead for PU-based ones.

3.4. Effect of scaffolds on cell growth and viability

Next, we wanted to investigate whether PMMA and PU supports can represent valuable tools to mimic the *in vivo* 3D context in which stromal cells proliferate in the bone marrow (BM). Human HS-5 stromal cells were seeded on top of the collagen-coated scaffolds and left to adhere and grow for 48 h. Nuclear staining with DAPI displayed very regularly shaped nuclei (Fig. 10), suggesting that both PMMA and PU supports do not affect cell adhesion and proliferation.

As shown in Fig. 11, the collagen coating procedure did not alter the porous architecture and the pore network remained open and interconnected. To check whether cells could effectively migrate inside the scaffold, immunofluorescence analysis was also performed. Confocal microscopy allowed to scan both sides of the scaffolds in depth. Fig. 12a clearly shows that cells not only seed on top of the scaffolds, but they also enter into the interconnected pore structure with a similar distribution into both PU and PMMA scaffolds. As expected, PU displayed a blue autofluorescence. Additionally, the analysis of the inner part of both PU and PMMA supports demonstrated the complete colonization by HS5 cells. What's more important, staining with Cy3-phalloidin made it possible not only to detect the expected fibroblast-like morphology, but also to confirm the presence of the very regular cytoskeleton, with large bundles of stress fibers as well as focal adhesions where cells attach to the scaffold (Fig. 12b, white squares).

The cytotoxic drug PF-04691502 is a dual phosphoinositide 3-kinase (PI3K) and mammalian target of rapamycin (mTOR) inhibitor, which has shown good cytotoxic activity towards primary effusion lymphoma cells (PEL) [35,36], but very low toxicity towards normal T and B lymphocytes, and is currently under evaluation in pre-clinical studies for cancer therapy. Here, we asked whether to grow stromal cells in adhesion on collagen-coated 3D supports, such as the PU or PMMA scaffolds described above, might stimulate their production of pro-survival factors and therefore help mimicking the physiological BM background. To do this, first we tested the viability of the Jurkat cell line upon addition for 24 h of vehicle or PF-04691502 at a concentration of 500 nM, either grown as single culture, in co-culture with HS-5 cells, or in co-culture with HS-5 cells previously seeded onto PMMA or PU scaffolds. Jurkat cell death in response to drug treatment in all the above conditions was evaluated by flow cytometry. The results are very clear: Jurkat cells as single culture displayed the expected 20% increased mortality following addition of the cytotoxic drug PF-04691502 to the growth medium, compared to their untreated counterpart (Fig. 13).

Conversely, the drug was not able to trigger HS-5 cells apoptosis, showing that this cell line is not sensitive to this molecule and should not therefore interfere with the cytotoxicity assay. However, when Jurkat and HS-5 cells were co-cultured, apoptosis was largely prevented both in basal culture condition and upon addition of the drug. This result was not unexpected, as stromal cells are indeed known to mimic, to some extent, the protective bone marrow microenvironment on cancer cells. Here, their pro-survival effect on Jurkat cells was easily detectable. Next, cell viability was monitored in cell co-cultures grown in the presence of either PMMA- or PU-based scaffolds. The results were comparable to that obtained in the absence of supports both in untreated and in PF-04691502-treated Jurkat/HS5 co-cultures. Interestingly, the result shows that the bone-marrow-mimicking, protective effect of stromal cells on Jurkat cancer cells is maintained, as the drug cytotoxicity is almost abrogated, when HS-5 cells are grown associated to the scaffolds. Therefore these devices can be very useful to test drug efficacy in a 3D-like microenvironment known to exert pro-survival effects on cancer cells.

4. Conclusions

The BM niche is the microenvironment where hematopoietic stem cells proliferate whilst keeping their cell state, and it is known to offer a protective setting for malignant cell survival and proliferation. The purpose of the present research was to produce 3D scaffolds that, mimicking the BM niche, could provide appropriate *in vitro* conditions to eventually test new treatments against hematological malignancies.

The production of scaffolds by means of SCPL was relatively easy and the appropriate choice of the polymer type, of the polymer-to-salt ratio and of the salt grain size allowed to control the porosity and the pore size, with immediate consequences on the mechanical properties of the scaffolds, whose elastic modulus under compression varied indicatively from 29 kPa for flexible PU-based samples (porosity: 91%) to 1283 kPa for rigid PMMA-based samples (porosity: 84%). According to the preliminary assays shown above, stromal cells not only adhere to the supports, upon collagen-coating, but they also retain their protective and pro-survival action towards co-cultured cancer cells, therefore preventing the cytotoxic effect of the drug. As it is very well known that efficacy of drug treatment can be mitigated, if not abolished, by the emergence of resistance mechanisms supported by components of the BM niche, it has become mandatory to test drug efficacy in pre-clinical settings that can reproduce as closely as possible the BM microenvironment. It is therefore possible to conclude that the SCPL technique, originally intended to produce scaffolds for bone tissue repair, can be successfully extended to the achievement of improved three-dimensional supports for stromal cells to mimic the BM niche.

Conflicts of interest

There are no conflicts to declare.

Acknowledgments

The research for this paper was financially supported by the Fondazione di Vignola, project "Utilizzo di tecnologia microfluidica e stampa 3d per la simulazione *in vitro* del microambiente stromale midollare" (year: 2016).

Prof. Carlo Palumbo is gratefully acknowledge for technical support in stereomicroscope imaging.

References

[1] X. Xu, M.C. Farach-Carson, X. Jia, Three-dimensional in vitro tumor models for cancer research and drug evaluation, Biotechnol. Adv. 32 (2014) 1256–1268, https://doi.org/10.1016/j.biotechadv.2014.07.009.

[2] M. Alemany-Ribes, C.E. Semino, Bioengineering 3D environments for cancer models, Adv. Drug Deliv. Rev. 79-80 (2014) 40–49, https://doi.org/10.1016/j.addr.2014.06.004.

[3] G. Rijal, W. Li, 3D scaffolds in breast cancer research, Biomaterials 81 (2016) 135–156, https://doi.org/10.1016/j.biomaterials.2015.12.016.

[4] M.E. Katt, A.L. Placone, A.D. Wong, Z.S. Xu, P.C. Searson, In vitro tumor models: advantages, disadvantages, variables, and selecting the right platform, Front. Bioeng. Biotechnol. 4 (12) (2016) 14, https://doi.org/10.3389/fbioe.2016.00012.

[5] D. Remick, Use of animal models for the study of human disease - a shock society debate (letter to the Editor), Shock 40 (2013) 345–346, https://doi.org/10.1097/SHK.0b013e3182a2aee0.

[6] N. Panoskaltsis, A. Mantalaris, J.H.D. Wu, Engineering a mimicry of bone marrow tissue ex vivo, J. Biosci. Bioeng. 100 (2005) 28–35, https://doi.org/10.1263/jbb.100.28.

[7] J. da Silva, F. Lautenschlager, E. Sivaniah, J.R. Guck, The cavity-to-cavity migration of leukaemic cells through 3D honey-combed hydrogels with adjustable internal dimension and stiffness, Biomaterials 31 (2010) 2201–2208, https://doi.org/10.1016/j.biomaterials.2009.11.105.

[8] T. Mortera Blanco, A. Mantalaris, A. Bismarck, N. Panoskaltsis, The development of a three-dimensional scaffold for ex vivo biomimicry, Biomaterials 31 (2010) 2243–2251, https://doi.org/10.1016/j.biomaterials.2009.11.094.

[9] N. Di Maggio, E. Piccinini, M. Jaworski, A. Trumpp, D.J. Wendt, I. Martin, Toward modeling the bone marrow niche using scaffold-based 3D culture systems, Biomaterials 32 (2011) 321–329, https://doi.org/10.1016/j.biomaterials.2010.09.041.

[10] O.S. Aljitawi, et al., A novel three-dimensional stromal-based model for in vitro chemotherapy sensitivity testing of leukemia cells, Leuk. Lymphoma 55 (2014) 378–391, https://doi.org/10.3109/10428194.2013.793323.

[11] E.G. Velliou, et al., Towards unravelling the kinetics of an acute myeloid leukaemia model system under oxidative and starvation stress: a comparison between two- and three-dimensional cultures, Bioprocess Biosyst. Eng. 38 (2015) 1589–1600, https://doi.org/10.1007/s00449-015-1401-z.

[12] V. Cannillo, F. Chiellini, P. Fabbri, A. Sola, Production of Bioglass® 45S5 - polycaprolactone composite scaffolds via salt-leaching, Compos. Struct. 92 (2010) 1823–1832, https://doi.org/10.1016/j.compstruct.2010.01.017.

[13] R. Huang, X. Zhu, H. Tu, A. Wan, The crystallization behavior of porous poly(lactic acid) prepared by modified solvent casting/particulate leaching technique for potential use of tissue engineering scaffold, Mater. Lett. 136 (2014) 126–129, https://doi.org/10.1016/j.matlet.2014.08.044.

[14] J.W. Kim, W.J. Ho, B.M. Wu, The role of the 3D environment in hypoxia-induced drug and apoptosis resistance, Anticancer Res. 31 (2011) 3237–3246.

[15] X. Liu, P.X. Ma, Polymeric scaffolds for bone tissue engineering, Ann. Biomed. Eng. 32 (2004) 477–486, https://doi.org/10.1023/B:ABME.0000017544.36001.8e.

[16] B. Dhandayuthapani, Y. Yoshida, T. Maekawa, D. Sakthi Kumar, Polymeric scaffolds in tissue engineering application: a review, Int. J. Polym. Sci. (2011) 19, https://doi.org/10.1155/2011/290602, 290602.

[17] D.A. Shimko, E.A. Nauman, Development and characterization of a porous poly(methyl methacrylate) scaffold with controllable modulus and permeability, J. Biomed. Mater. Res., Part B 80B (2007) 360–369, https://doi.org/10.1002/jbm.b.30605.

[18] H. Janik, M. Marzec, A review: fabrication of porous polyurethane scaffolds, Mater. Sci. Eng. C 48 (2015) 586–591, https://doi.org/10.1016/j.msec.2014.12.037.

[19] H. Khatoon, S. Ahmad, Polyurethane: a versatile scaffold for biomedical applications, Significances Bioeng. Biosci. 2 (2018) 3, https://doi.org/10.31031/SBB.2018.02.000536, SBB.000536.2018.

[20] PMMA Technical Data Sheet, in: http://www.plaskolite.com/PolymerCatalog/CA-1000-I.

[21] PU Technical Data Sheet, in: http://www.biomertechnology.co.uk/uploaded/categories_24_96.pdf.

[22] R. Hoogenboom, R. Becer, C. Guerrero-Sanchez, S. Hoeppener, U.S. Schubert, Solubility and thermoresponsiveness of PMMA in alcohol-water solvent mixtures, Aust. J. Chem. 63 (2010) 1173–1178, https://doi.org/10.1071/CH10083.

[23] L. Goers, P. Freemont, K.M. Polizzi, Co-culture systems and technologies: taking synthetic biology to the next level, J. R. Soc. Interface 11 (2014) 20140065, https://doi.org/10.1098/rsif.2014.0065.

[24] N.M. Maraldi, et al., Phosphoinositidase C isozymes in SaOS-2 cells: immunocytochemical detection in nuclear and cytoplasmic compartments, Biol. Cell. 79 (1993) 243–250, https://doi.org/10.1016/0248-4900(93)90143-3.

[25] M. Zavatti, et al., Development of a novel method for amniotic fluid stem cell storage, Cytotherapy 19 (2017) 1002–1012, https://doi.org/10.1016/j.jcyt.2017.04.006.

[26] S. Bose, M. Roy, A. Bandyopadhyay, Recent advances in bone tissue engineering scaffolds, Trends Biotechnol. 30 (2012) 546–554, https://doi.org/10.1016/j.tibtech.2012.07.005.

[27] J. Zhang, L. Wu, D. Jing, J. Ding, A comparative study of porous scaffolds with cubic and spherical macropores, Polymer 46 (2005) 4979–4985, https://doi.org/10.1016/j.polymer.2005.02.120.

[28] D.C. Sin, et al., Polyurethane (PU) scaffolds prepared by solvent casting/particulate leaching (SCPL) combined with centrifugation, Mater. Sci. Eng. C 30 (2010) 78–85, https://doi.org/10.1016/j.msec.2009.09.002.

[29] K. Gorna, S. Gogolewski, Biodegradable porous polyurethane scaffolds for tissue repair and regeneration, J. Biomed. Mater. Res. A 79A (2006) 128–138, https://doi.org/10.1002/jbm.a.30708.

[30] L. Safinia, N. Datan, M. Höhse, A. Mantalaris, A. Bismarck, Towards a methodology for the effective surface modification of porous polymer scaffolds, Biomaterials 26 (2005) 7537–7547, https://doi.org/10.1016/j.biomaterials.2005.05.078.

[31] V. Karageorgiou, D. Kaplan, Porosity of 3D biomaterial scaffolds and osteogenesis, Biomaterials 26 (2005) 5474–5491, https://doi.org/10.1016/j.biomaterials.2005.02.002.

[32] B. Stuart, Infrared Spectroscopy: Fundamentals and Applications, John Wiley & Sons, Inc., 2004.

[33] L.G. Gibson, M.F. Ashby, The mechanics of three-dimensional cellular materials, Proc. R. Soc. Lond. A 382 (1982) 43–59, https://doi.org/10.1098/rspa.1982.0088.

[34] C. Jo, J. Fu, H.E. Naguib, Constitutive modeling for characterizing the compressive behavior of PMMA open-cell foams, J. Polym. Sci. B Polym. Phys. 45 (2007) 436–443, https://doi.org/10.1002/polb.21037.

[35] L. Mediani, et al., Reversal of the glycolytic phenotype of primary effusion lymphoma cells by combined targeting of cellular metabolism and PI3K/Akt/mTOR signaling, Oncotarget 7 (2016) 5521–5537, https://doi.org/10.18632/oncotarget.6315.

[36] J. Bertacchini, et al., Feedbacks and adaptive capabilities of the PI3K/Akt/mTOR axis in acute myeloid leukemia revealed by pathway selective inhibition and phosphoproteome analysis, Leukemia 28 (2014) 2197–2205, https://doi.org/10.1038/leu.2014.123.